Age-related myelin deficits in the auditory brain stem contribute to cocktail-party deficits

S. Poleg*[1], B.Z. Li*[1], M. Ridenour[1], E.G. Hughes[2], D.J. Tollin[1], and A. Klug[1]
* indicates equal contribution

1 = Department of Physiology & Biophysics, University of Colorado School of Medicine, Aurora, Colorado, USA.

2 = Department of Cell and Developmental Biology, University of Colorado School of Medicine, Aurora, Colorado, USA.

Financial disclosures/conflicts of interest:
This work was funded by NIH-NIDCD R01 DC017924 (MPIs: Tollin and Klug). Imaging was performed in the Advanced Light Microscopy Core Facility of the NeuroTechnology Center at the University of Colorado Anschutz Medical Campus, which is supported in part by Rocky Mountain Neurological Disorders Core Grant (P30 NS048154) and by Diabetes Research Center Grant (P30 DK116073).

Acknowledgements:
We would like to thank Dr. Anza Darehsouri for help with electron microscopy, Mr. Carol Mirita and Dr. Dominik Stich for help with CARS microscopy, and Dr. Tim Lei for designing and writing the software used to measure auditory brain stem responses. We would also like to thank Dr. Alon Poleg-Polsky for many helpful discussions and for support with the oligodendrocyte imaging and quantification.

Author Contributions:
S.P., B.Z.L., M.R. designed study, collected data, analyzed data, performed modeling. E.G.H., D.J.T. and A.K. conceived of study, designed experiments.

All correspondence and materials requests should be addressed to:
Achim Klug, PhD, Department of Physiology & Biophysics,
Research Complex 2, Rm 9120, MS 8625, 12700 E. 19th Avenue, University of Colorado School of Medicine, Aurora, CO 80045, USA.
E-mail: achim.klug@CUAnschutz.edu,
Phone: 303-724-4621.

ABSTRACT

Age-related hearing loss is a global health problem of increasing importance. While the role of peripheral hearing loss is well understood and treatments are available, central hearing loss, the ability of the brain to make sense of sound, is much less well understood and no treatments are available. We report on age-related alterations in the auditory brain stem which compromise a listener's ability to isolate a sound from competing background noises, for example in a crowded restaurant. Sound localization depends on extreme temporal precision on the order of microseconds, and the sound localization pathway shows several specializations towards temporal precision. The pathway from the cochlear nucleus to the medial nucleus of the trapezoid body (MNTB) is heavily myelinated and terminates in the calyx of Held. Using auditory brain stem response measurements (ABRs), we found that the physiological properties of MNTB changes with age. The mechanism is that in older animals, MNTB afferents demyelinate to various degrees, resulting in larger variability in the timing of responses. Myelin is produced by oligodendrocytes, and we found that fewer mature, but more precursor and immature oligodendrocytes are present in MNTB of aged animals, suggesting that the demyelination is an age-related deficit in oligodendrocyte maturation.

INTRODUCTION

Age-related hearing loss, or presbycusis, is a global health problem which is becoming more important as many modern societies have progressively larger portions of aging members. Presbycusis affects approximately one-third of adults starting in middle age, with over half of adults aged 70 and older experiencing it[1–4]. Additionally, untreated hearing loss has a significant impact on the quality of life, because in addition to the direct impact of the hearing loss itself, it is linked to an elevated risk of secondary conditions such as depression, social isolation, dementia, Alzheimer's disease and many other mental health problems[2,5–9]. Thus, early detection and treatment of hearing loss are crucial for promoting healthy aging.

Peripheral hearing loss – the loss of hair cells in the inner ear – is one mechanism which contributes to presbycusis. As hair cells die during the lifetime of humans or other mammalian species, the thresholds for the detection of sound increase. This form of hearing loss has been known for several decades and treatments such as hearing aids or cochlear implants are common and fairly effective in most cases [10].

By contrast, a completely independent mechanism of age-related hearing loss is mediated by changes of neural circuits in the CNS, here termed "central hearing loss". In contrast to peripheral hearing loss, central hearing loss is much less well understood and no treatments are available to date. While changes in several locations along the ascending auditory pathway have been suggested to contribute to central hearing loss, one major component involves the age-related reduction in sound localization abilities despite subjects having normal hearing thresholds[11–14].

The ability to pinpoint the source of a sound relies on a precise comparison of inputs from both ears[15]. Especially for low-frequency sound localization, extreme temporal precision is required because the brain needs to detect differences in arrival time of the same sound wave between the two ears which are on the order of just a few microseconds, thus one to two orders of magnitude faster than a typical action potential [16]. To accomplish such high levels of precision, this process depends on a number of specializations along the sound localization pathway, one of which is fast synaptic transmission along heavily myelinated axons in the brainstem[16–18]. The medial nucleus of the trapezoid body (MNTB), which provides fast and temporally precise glycinergic inhibition to the principal sound localization nuclei, the lateral and medial superior olive (LSO and MSO, respectively), stands out for having both one of the largest synapses in the brain (the calyx of Held) and wide-diameter afferent axons, reflecting the critical need for temporal precision in this circuit[18–22].

It seems intuitive that even minor disruptions in the temporal precision in this pathway could lead to significant impairment in the encoding of the cues to sound location by the LSO and MSO and thus difficulties in behavioral tasks that rely on binaural information, such as detecting speech in noise and sound localization. Alterations in myelination within the auditory brainstem affect the speed of electrical propagation and, consequently, the timing of auditory brainstem activity[18,20,23–25]. Evidence from various studies indicates that myelination deficiencies contribute to the aging brain phenotype[26,27], begging the question whether age-related myelination deficits

might contribute to a decline in timing within the sound localization pathway, which in turn might contribute to presbycusis. Binaural hearing is known to mediate not only sound localization abilities per se but also help a listener in acoustically busy environments such as crowded restaurants where multiple sound sources are active simultaneously while a listener typically wants to focus on a single sound source such as the voice of a conversation partner. In such situations, often termed "cocktail party situations", the sound localization circuit helps us to isolate the sound source of interest from distracting background noises based on spatial location[28–30]. Thus, a listener affected by age-related decline in spatial hearing should primarily notice a decline in their abilities to focus on a sound of interest within background noises[14].

The decline in temporal processing associated with aging is not unique to humans; rather, it appears to be a widespread phenomenon among mammals[31,32]. The Mongolian gerbil (*Meriones unguiculatuns*) is often used as an animal model for human hearing, including age-related alterations in the sound localization pathway. Gerbils possess distinctive features such as well-developed low-frequency hearing and low frequency sound localization abilities[33] while exhibiting minimal age-related loss of hair cells in the inner ear[34,35]. This renders them better models for studying human hearing compared to other rodents, such as mice and rats[36,37].

In our study, we employ a combination of electrophysiological assessments of auditory circuits, immunohistochemistry, electron microscopy (EM) and coherent anti-stokes Raman spectroscopy (CARS) to investigate the contribution of the myelin microstructure in aging gerbils compared to young adult controls[38,39]. We found significantly attenuated wave-III and earlier onset wave-IV in the click ABRs from old gerbils, suggesting degradation of inhibitory inputs and MNTB activity in the superior olivary complex.

In addition, the MNTB of aging gerbils exhibits significantly reduced myelin thicknesses and axon diameters, leading to suboptimal action potential transduction. To uncover potential mechanisms underlying alterations in myelin structure, we investigated the numbers of mature and precursor oligodendrocytes (OLs and OPCs). Our results demonstrate a deficit in OPC maturation in old gerbils, without a change in the total number of oligodendrocytes, suggestive of a potential explanation through which auditory phenotypes might arise in aging.

Results

The goal of this study was to test the hypothesis that age-related alterations in the auditory brainstem contribute to decreased performance in acoustic environments with multiple simultaneous sounds. We used Mongolian gerbils as our model, with young (2-3 months old) and aged animals (2.5 to 3.5 years old). All experiments were conducted on the same cohort of animals to determine if physiological responses correlated with histological findings.

Electrophysiology

To test the physiological responses of the auditory brain stem to sound, we performed auditory brain stem response (ABR) recordings, a non- or minimally invasive method that measures the compound activity of neurons in lower auditory centers in response to brief sound stimuli. As neural responses to these sound stimuli ascend the auditory pathway, they create a series of peaks (waves) that represent activity in these centers. In gerbils, wave I is mediated by the spiral ganglion neurons, wave II is generated by the cochlear nucleus, wave III is largely mediated by the medial nucleus of the trapezoid body (MNTB), wave IV is formed by lateral and medial superior olive, and wave V is contributed by the lateral lemniscus and inferior colliculus.

Five distinct ABR waves were present in most young (Figure 1A) and old gerbils (Figure 1B) when click stimuli were used. There was no significant difference in click ABR thresholds between young (N = 62) and old gerbils (N = 30) by using either automated algorithms to determine ABR thresholds (Young: 32.01 ± 12.71 dB SPL (mean ± SD); old: 29.86 ± 12.00 dB SPL; U = 1014.5, P = 0.4841 for a two-sided Mann–Whitney U test) (Figure 1C) or manual inspection by an observer blinded to the experimental condition (Young: 31.13 ± 13.92 dB SPL; old: 34.00 ± 14.28 dB SPL; U = 872.5, P = 0.6271 for a two-sided Mann–Whitney U test) (Figure 1D). The occurrence of ABR waves increased with the click sound levels in both groups (Figure 1E-F), however, the young gerbils showed a relatively higher probability of occurrence of wave I at high sound levels (young: 83.87% at 90 dB SPL; old: 73.33% at 90 dB SPL) and wave III at a medium sound level (young: 82.26% at 60 dB SPL; old: 66.67% at 60 dB SPL). These differences imply that aging may affect cochlear and potentially also MNTB activity at least to some extent.

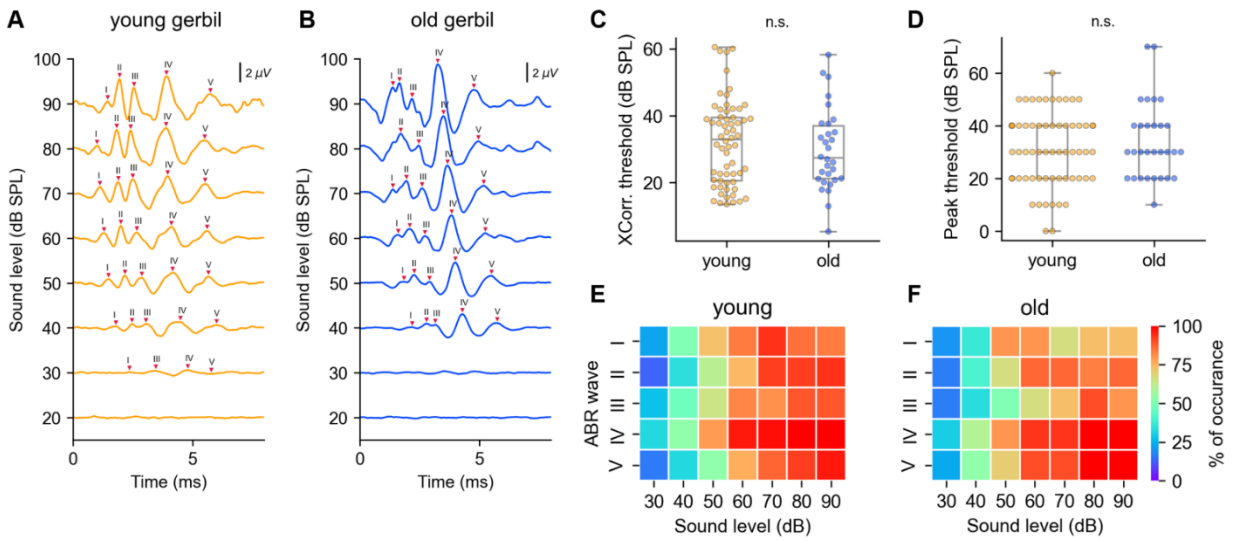

Figure 1. *Click ABR traces, thresholds and detected waves in young and old gerbils.* ***(A)*** *Example ABR traces recorded from a young gerbil (P85) elicited by click stimuli at different intensity levels.* ***(B)*** *Example ABR traces from an old gerbil (P757).* ***(C)*** *Cross correlation thresholds of click ABRs between young and old gerbils calculated using sigmoid function fitting on signal cross-correlations. (Young: 32.01 ± 12.71 dB SPL (mean ± SD); old: 29.86 ± 12.00 dB SPL (mean ± SD); U = 1014.5, P = 0.4841 for a two-sided Mann–Whitney U test)* ***(D)*** *Peak thresholds derived from a semi-automatic peak detection used by blinded observers (Young: 31.13 ± 13.92 dB SPL (mean ± SD); old: 34.00 ± 14.28 dB SPL (mean ± SD); U = 872.5, P = 0.6271 for a two-sided Mann–Whitney U test).* ***(E-F)*** *Probability of occurrence of a particular ABR wave at a particular sound intensity when click sounds were used with young gerbils* ***(E)*** *and old gerbils* ***(F)****.*

Several metrics of the five waves are plotted in Figure 2. On average, old gerbils exhibited significantly attenuated wave I and wave III amplitudes (Figure 2A), and significantly narrower wave III peak half-widths (Figure 2B) at most sound levels, indicating weaker cochlear responses and potentially also MNTB activity. Regarding peak latency, most waves showed no significant difference between young and old gerbils, however wave IV was significantly advanced in old gerbils at sound levels less than 80 dB SPL (Figure 2C). Further analysis on the peak intervals between ABR waves revealed significantly shortened wave II-IV interval in old gerbils at all sound levels (Figure 2D), implying degradation of inhibitory activities between cochlear nucleus and superior olive.

The mean wave I-V and reconstructed click ABRs of young and old gerbils are illustrated in Figure 3, demonstrating the trend of aging effects across all samples. Wave I and wave III were largely attenuated and wave IV was advanced in old gerbils, but other waves were mostly consistent between young and old animals. Despite the differences in wave I amplitude, the peak metrics of wave II remain unchanged, which could be caused by latent neural plasticity in the

cochlear nucleus that compensates for hearing loss. Additional aging-related changes were observed in the form of degraded wave III response and underlying MNTB activity.

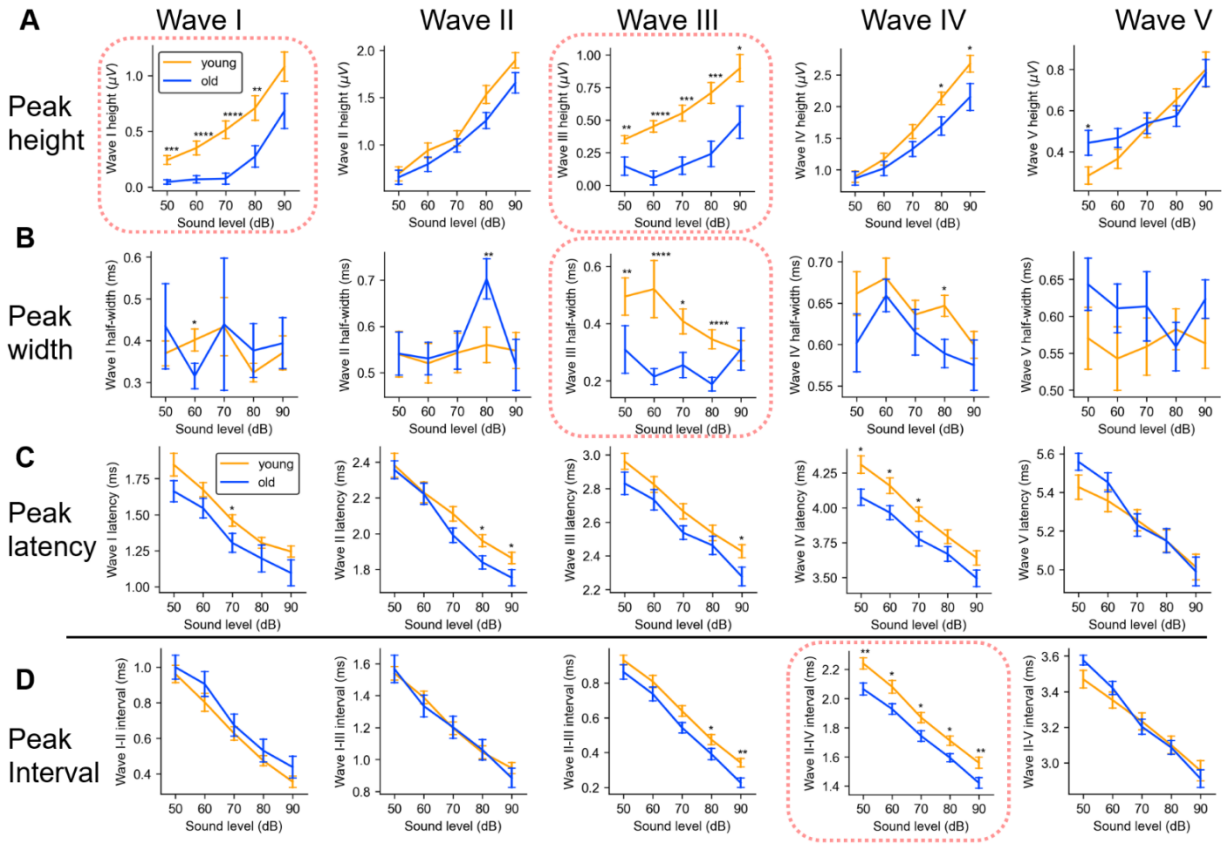

Figure 2. *Peak metrics of ABR waves detected with clicks vs sound levels between young (N=62; orange lines) and old (N=30; blue lines) gerbils using Mann-Whitey U test (*: p<0.05; **: p <0.01; ***: p<0.001; ****: p<0.0001; red dash lines: waves with significantly different metrics over more than 4 sound levels).* ***(A)*** *Peak height.* ***(B)*** *Peak half-width.* ***(C)*** *Peak latency.* ***(D)*** *Time interval between wave peaks.*

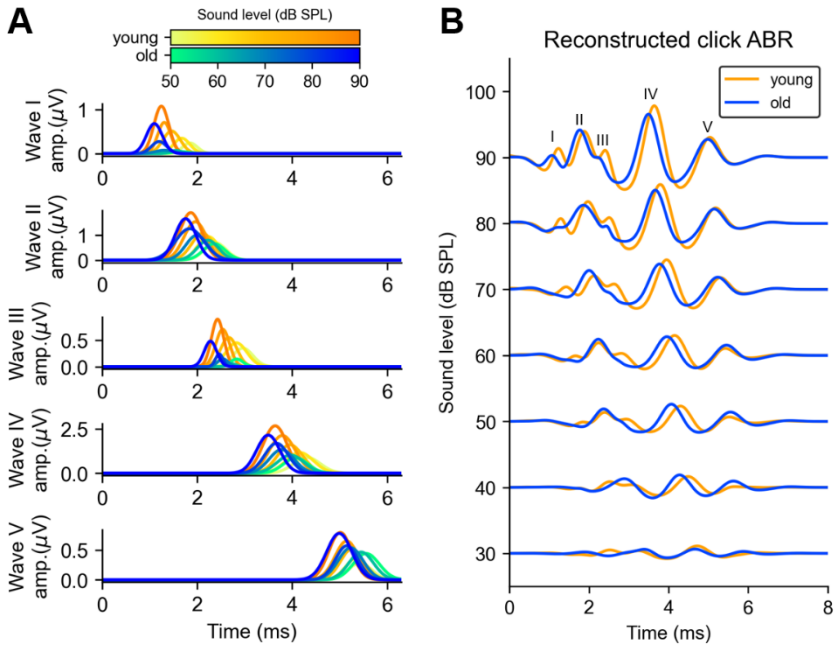

Figure 3. *Reconstructed ABR waves* ***(A)*** *and click ABRs* ***(B)*** *based on average peak metrics from young (orange lines) and old gerbils (blue lines).*

CARS images

After establishing the electrophysiological abnormalities in the aging gerbil auditory brainstem, we hypothesized that these abnormalities could be attributed to changes in axonal conductance because previous work has shown the potential for myelination plasticity throughout life[40,41]. Using CARS microscopy[38,39], we first measured the axonal diameter of putative globular bushy cell axons in the auditory brainstem that innervate the MNTB and form the calyx of Held. In both young and old gerbils, the MNTB was sampled with multiple z-stack images, which were subsequently analyzed for axon thickness (Figure 4). We found a profound difference in axon width between the two age groups: the mean (±SD) axon diameter in young gerbils measured 3.9 ± 0.18 (n=10), whereas in old gerbils it was reduced to 2.9 ± 0.18 (n=7, $p<0.0001$, t-test, Figure 4C).

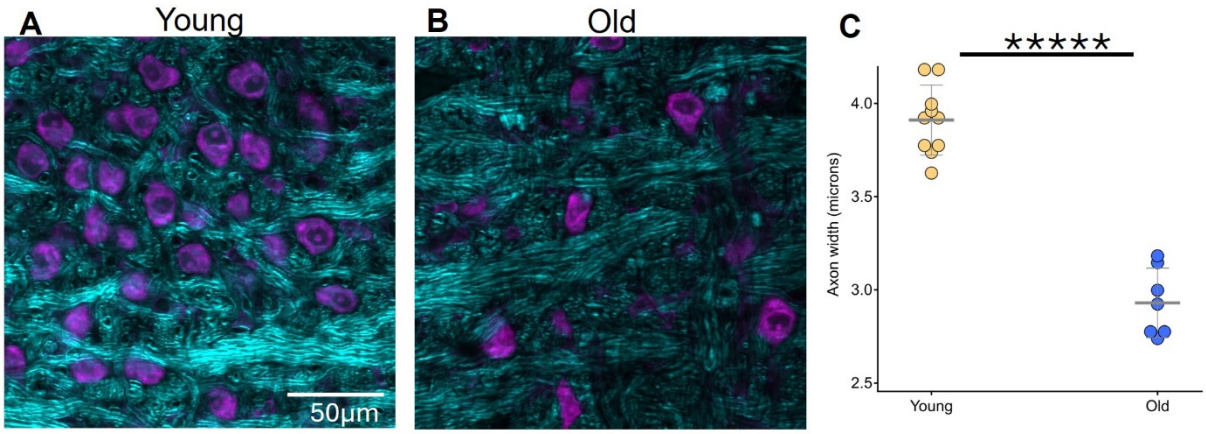

Figure 4 *: Fiber diameter size is reduced in old gerbils. Representative MNTB images show cell bodies stained with Nissl (purple) and CARS signal (cyan) in young* ***(A)*** *and old* ***(B)*** *gerbils.* ***(C)*** *Box plots represent data from individual animals (n=10 young, n=7 old, with 30 measurements per section and 2–6 sections per animal). ****p = 7e-8*

EM images

For EM images, cross-sections of myelinated fibers were blindly sampled through visual inspection. The myelin layers were semi-automatically segmented by active contours. The morphological metrics, including fiber diameter, myelin thickness, axon diameter, and g-ratio were extracted as shown in Figure 5B. A total of 3027 myelinated axons were sampled and quantified in 133 EM images captured from 6 gerbils (Young: n_{axon} = 1266, N_{animal} = 4; Old: n_{axon} = 1761; N_{animal} = 2). The two groups presented several differences in the cross-section of axon fibers (Figure 6A), with young gerbils containing thicker axon fibers with clearer and better defined myelin layers. Similar as with CARS, we found age-related changes, in particular a reduction in fiber diameter (Figure 6D; young: 2.948 ± 1.22 µm (mean ± SD), old: 2.349 ± 1.271 µm; $P < 0.0001$, Mann–Whitney U test) and myelin thickness (Figure 6E; young: 0.608 ± 0.242; old: 0.561 ± 0.304 µm; $P < 0.0001$, Mann–Whitney U test). Thus, the average fiber diameter was significantly decreased by about 0.6 µm, and the myelin thickness decreased by around 0.05 µm.

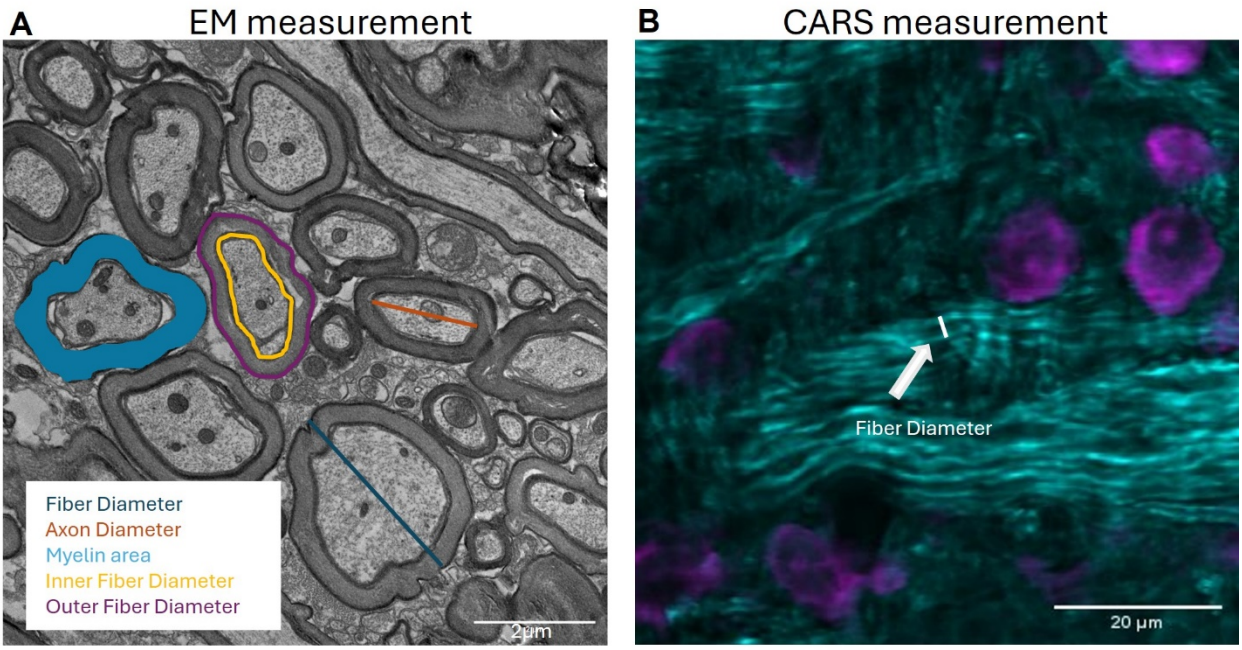

Figure 5: Quantification of myelination morphology in CARS and EM images. EM images provide higher resolution for detailed analysis, including fiber diameter (dark blue), axon diameter (teal), myelin thickness (green), inner (orange), and outer (purple) fiber diameter **(A).** CARS images were quantified using the FIJI line segment tool; a white line **(B)** was drawn, and the measure function was used to determine fiber diameter for 20 axons per image (Nissl-stained cell bodies in purple, CARS signal in cyan).

We estimated the physiological effects of this partial demyelination with a myelinated axon model[18,42] and found a slower conduction velocity of the action potential propagation along the axon (Figure 6F; young: 12.224 ± 5.90 m/s; old: 10.145 ± 6.783 m/s; $P < 0.0001$, Mann–Whitney U test), and thus the fiber conduction velocity slowed by 1.081 m/s. . However, these metrics displayed skewed distributions (Figure 6B,C), and the centroids of the histograms were clearly separated with median differences of 0.685 µm in fiber diameter, 0.073 µm in myelin thickness, resulting in 2.703 m/s in conduction velocity per the models. Note that the larger variations in the EM fiber metrics of the old animals (Figure 6D-F) translated with our model into an increased standard deviation of the conduction velocity, suggesting a relatively larger variation of transmission latencies in the old group (± 204 µs for 3-mm distance) compared to the young group (± 177 µs for 3-mm distance). Consequently, the axon fibers of old gerbils likely show degraded action potential propagation with longer and more variable transmission latencies. By calculating the time course of action potential propagation through a 3-mm axon fiber with conduction velocities between the 25% to 75% quartile levels, we calculated that approximated transmission latencies range from 0.20 to 0.37 ms in young gerbils and from 0.24 to 0.52 ms in old gerbils.

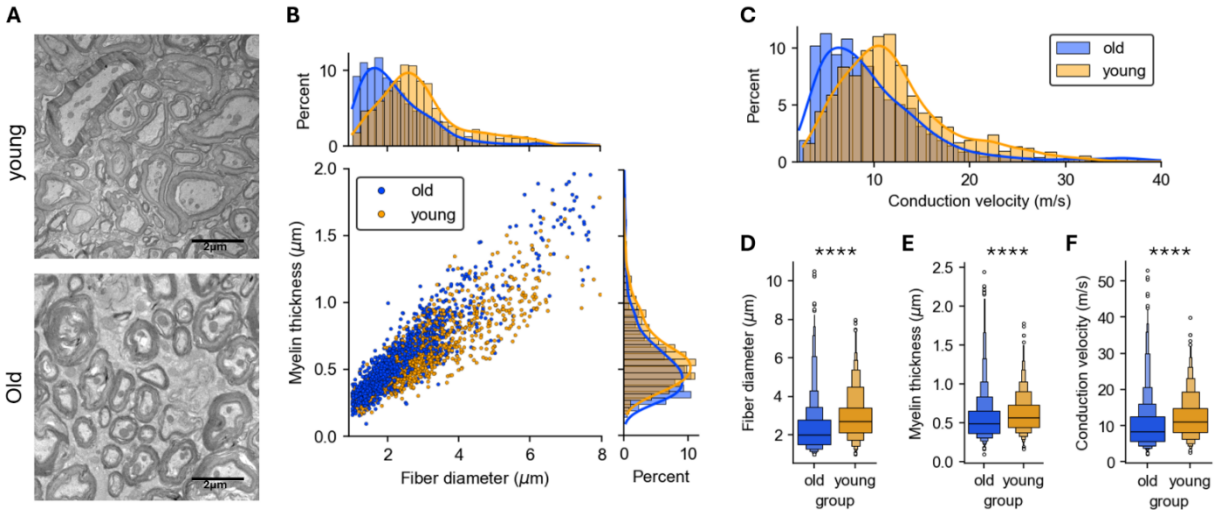

Figure 6. Myelination properties acquired from EM images. (A) *Example EM images captured from a young gerbil (top) and an old gerbil (bottom). (error bar: 2 μm)* ***(B)*** *Fiber diameter and myelin thickness of quantified axon fibers sampled from the young group (n_{axon} = 1266; N_{animal} = 4) and the old group (n_{axon} = 1761; N_{animal} = 2).* ***(C)*** *Distribution of the fiber conduction velocity estimated by simulating the action potential propagation along myelinated axons.* ***(D)*** *Fiber diameters in two groups (Young: 2.948 ± 1.22 μm (mean ± SD), 2.707 μm (median); Old: 2.349 ± 1.271 μm (mean ± SD), 2.022 μm (median); P < 0.0001 in the two-sided Mann–Whitney U test).* ***(E)*** *Myelin thickness in two groups (Young: 0.608 ± 0.242 μm (mean ± SD), 0.563 μm (median); Old: 0.561 ± 0.304 μm (mean ± SD), 0.49 μm (median); P < 0.0001 in the two-sided Mann–Whitney U test).* ***(F)*** *Estimated fiber conduction velocity in two groups (Young: 12.224 ± 5.90 m/s (mean ± SD), 11.143 m/s (median); Old: 10.145 ± 6.783 m/s (mean ± SD), 8.435 m/s (median); P < 0.0001 in the two-sided Mann–Whitney U test).*

Oligodendrocytes counts

Using EM and CARS microscopy, we identified an age-dependent decrease in myelination. Oligodendrocytes (OLs) are specialized glia cells responsible for producing myelin which insulates axons in the central nervous system, and their loss can lead to changes in myelination in MNTB[39]. To investigate whether structural changes are linked to alterations in the quantity of mature (OL) and precursor oligodendrocytes (OPC), we employed an immunohistochemical method. Representative z-stacks of aspartoacylase (ASPA) and sex determining region Y-box 10 (SOX-10) labeled MNTB tissue were imaged with a confocal microscope. SOX-10 serves as a marker for the entire OL lineage (OPC + OL), whereas ASPA specifically identifies mature OLs. Thus, cells solely stained for SOX-10 represent OPCs, while co-staining with ASPA indicates mature OLs (Figure 7). Our initial focus was on comparing the density and maturation status of MNTB OLs across different age groups.

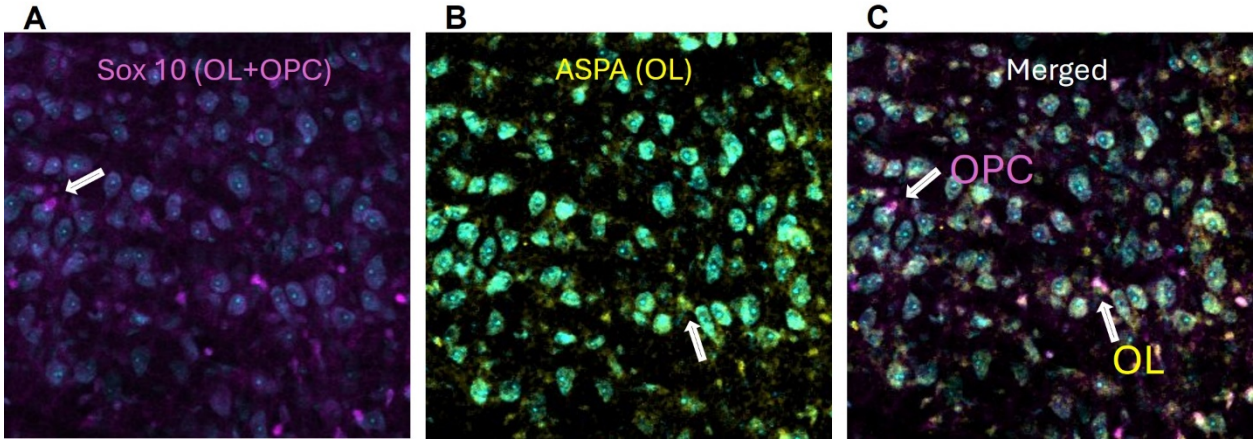

***Figure** 7: Differentiation of Oligodendrocytes (OLs) and Oligodendrocyte Precursor Cells (OPCs); **(A)** Sox-10, a marker for the entire OL lineage (OPCs and OLs), is labeled in magenta **(B)** ASPA, a specific marker for mature OLs, is shown in yellow. **(C)** OPCs were measured from cells labeled with Sox-10 but not ASPA. Mature OLs express both markers. MNTB cell bodies are indicated in cyan. Labeling was thresholded before analysis.*

We found a significant reduction in OL count within the aging population (1050 ± 157 vs 683 ± 210 cells / MNTB, p=0.004, Figure 8), despite the total cell count (OL plus precursor plus immature oligodendrocytes) remaining relatively consistent (Figure 8). This discrepancy may suggest impairment in OPC maturation among aged animals.

The MNTB tonotopic axis encodes high to low sound frequencies across the medial to lateral dimension. Previous research found that parameters such as soma size, synaptic properties and myelination change along this tonotopic axis[18,20,43]. Accordingly, we assessed OL in three MNTB divisions: medial (high frequency), central (intermediate frequency) and lateral (low frequency)[39]. We found a substantial reduction in OL number in old gerbils within each section (Figure 8C), but no significant changes in cell counts or types[18] between the tonotopic regions (Figure 8C, D).

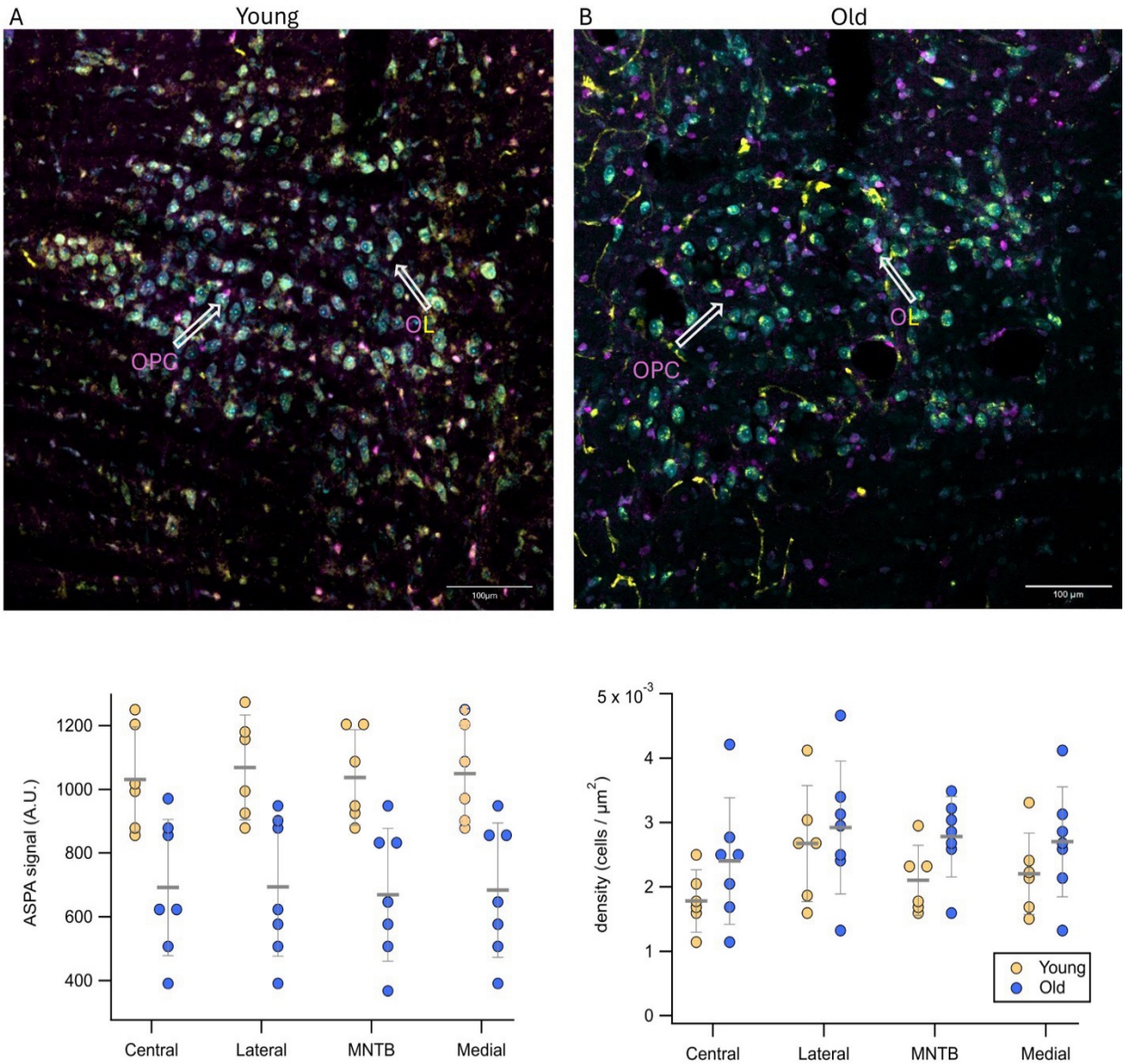

Figure 8: *Oligodendrocyte (OL) numbers decrease compared to oligodendrocyte precursor cells (OPC), in the MNTB of old gerbils. Representative images show OLs (ASPA/sox-10 marker in yellow/magenta) and OPCs (sox-10 without ASPA staining) in young* ***(A)*** *and old* ***(B)*** *gerbils.* ***(C)*** *ASPA fluorescence levels for young (yellow, n=6) and old (blue, n=6) gerbils across total, medial, center, and lateral MNTB. * $p<0.05$ using ttest and Bonferroni correction for multiple comparisons. No difference was found across MNTB tonotopic areas within each age group. (D) OL density in MNTB is similar in both age groups.*

DISCUSSION

We report four main findings: First, physiological responses of the auditory brain stem, specifically nuclei of the sound localization pathway, change with age. The largest changes we observed in ABR recordings were wave III changes with age. Wave III largely reflect neural activity in the MNTB, thus the changes in this wave indicate age related changes with MNTB physiology. Importantly, while we also found age-related changes in wave I, the observed changes in wave III seem to be independent rather than a simple reflection of the wave I changes. Second, the exceptionally heavily myelinated afferent axons to MNTB show age-related decreases in myelination, both with CARS and with EM imaging. Third, when the physiological consequences of the observed decreases in myelination were modeled, the modeling results were consistent with the data on age-related changes in the ABR recordings, indicating that the reduced myelination is a main factor in this altered physiology. Fourth, the number of mature oligodendrocytes was reduced in old gerbils, consistent with the reduction in myelination. However, the *total* number of oligodendrocytes was unchanged, suggesting an age-related impairment in oligodendrocyte maturation.

We suggest that the wave I reductions cannot explain the wave III reductions, because wave II was unchanged between young and old animals. In other words, any peripheral hearing loss that the older animals may have experienced was not measurable at the level of the cochlear nucleus. The most likely reasons for this are compensatory mechanisms which upregulate auditory gain. Such mechanisms are commonly observed in many forms of hearing loss and might explain why wave II amplitudes were similar between young and old animals[44]. If that is the case, the wave III reductions observed in old animals must have a mechanism which is at least partially independent of peripheral hearing loss.

The mammalian sound localization pathway critically depends on very accurate timing of information[16]. Sound localization is a computational process which relies on the comparison of arrival time and intensity of the same sound wave between the two ears. Low frequency sounds are localized by the interaural time difference, which can be as small as only several tens of microseconds at the system's localization threshold, thus about two orders of magnitude faster than a typical action potential[16,45]. Not surprisingly, there are many specializations towards the processing of neural information with very high levels of temporal fidelity. The perhaps most extreme specializations can be found in the pathway of the MNTB. MNTB neurons feature several adaptations to process information with very high levels of temporal fidelity. One such adaptation is the calyx of Held[46,47], a type of giant synapse which innervates the MNTB principal cell body. Furthermore, MNTB neurons have small dendrites, are electrically very compact, have large synaptic currents, a low input resistance, kinetically fast receptors, just to name a few of these subcellular specializations[17,48,49]. The most likely functional significance of all these specializations is speed and temporal fidelity in MNTB activity, which is obviously required by the neural targets of MNTB. The target nuclei of MNTB include but are not limited to the principal sound localization nuclei, the lateral and medial superior olive (LSO and MSO respectively)[50]. Since MNTB neurons are glycinergic [51,52], the role of MNTB within the sound localization process

is to provide fast and well-timed neural inhibition to the sound localization process, which itself is critically dependent on temporal precision.

In this context it seems intuitive that afferent axons to MNTB also need to be capable of transmitting neural activity quickly and with high temporal fidelity. These axons are therefore exceptionally thickly myelinated and additionally, the spacing and size of the nodes and internodes is tightly controlled to accomplish particular action potential propagation time constants[18,20]. Moreover, sound elicited neural activity in this pathway has been shown to contribute to the establishment of these tight parameters in an activity dependent way during postnatal development[25].

Our results indicate that this axon population partially demyelinates during aging. Equally important, the population of axons in older animals has a wider distribution of myelination levels, i.e. some axons are more demyelinated than others. The partial demyelination should lead to reduced capabilities to conduct action potentials as well as increased jitter in these fibers, with the result that the high level of temporal fidelity in these afferents is lost. Additionally, normal aging has been associated with a (partial) loss of myelin in other neural systems, and remyelination can result in shorter internode length, which would also decrease the action potential propagation speed and additionally compromise the extreme temporal fidelity and precision that was established in this system during early postnatal development, and that is required for accurate sound localization[53]. Our model-estimated conduction velocity based on myelination data from EM images further supports this idea by suggesting an increased variability of the fiber conduction velocity and prolonged transmission latencies in older animals.

What might be the mechanisms for this age-related demyelination of the MNTB afferent fiber bundle? One possibility is that general age-related myelin degeneration and incomplete regeneration may play a role here, as has been demonstrated in other neural systems[53,54]. Our results also show a decrease in mature oligodendrocytes in aged animals, which would be consistent with incomplete myelin repair[73]. Interestingly, while we observed an age-related decrease in mature oligodendrocytes, the total number of oligodendrocytes was comparable to young animals, suggesting that incomplete maturation of new oligodendrocytes during the animal's lifetime might be an important mechanism of myelin degeneration with age.

Another well-described age-related change in the peripheral auditory system is synaptopathy – the progressive loss of auditory nerve fiber synapses with age. While this loss may not necessarily lead to increased auditory thresholds, it certainly leads to decreased activity levels in downstream auditory areas such as the cochlear nucleus and MNTB[55,56]. Potentially, this reduced activity may contribute to reduced myelination. One mechanism for reduced activity in brainstem neurons might be caused by the loss of subthreshold inputs to cochlear nucleus bushy cells from auditory nerve due to synaptopathy. It is well known that convergence of auditory nerve fibers onto cochlear nucleus bushy cells is important for the emergence of precise coding of both temporal fine structure and envelope cues in the brainstem for suprathreshold sounds[71]. Computational modeling by Budak et al (2022) demonstrates that synaptopathy comparable to that found empirically in animal models leads to significant lowering of overall spike rate in globular (GBC) and spherical (SBC)

bushy cells of the cochlear nucleus as well as the medial superior olive (MSO) by anywhere from 30-70%! SBCs from both ears provide excitatory inputs to the MSO, which encodes low-frequency fine structure interaural time differences (ITDs). SBCs provide the excitatory input to the lateral superior olive (LSO) from the ipsilateral ear while GBCs from the contralateral ear provide inhibitory input via a synapse through the MNTB. Budak[72] also showed that synaptopathy significantly reduced phase locking in SBCs and GBCs and thus the ability of the simulated MSO to encode the ITD cue was severely degraded. Our finding here of age-related reductions in myelin in brainstem axons despite no significant hearing loss is consistent with a hypothesis that activity-dependent reductions in spiking of cochlear nucleus bushy cells as well as phase locking due to synaptopathy[72] leads to reduced myelin. Reduced myelin would be expected to lead to increased spike jitter and thus poorer temporal encoding of sound, which in turn would cause substantial deficits in the encoding of the acoustical cues to sound location by neurons in the MSO and LSO. This, then, would be expected to cause difficulties in binaural and spatial hearing behavioral tasks, such as sound localization or listening in noisy environments.

Consistent with this view are recent results from oligodendrocytes in the developing auditory system, which show that one population of these cells contains voltage gated sodium channels, is excitable, and that excitation of this population supports maturation of these cells[57]. While a parallel role in aging has not been shown, it seems possible that reduced activity from the auditory nerve may further contribute to the impaired oligodendrocyte maturation and, by extension, the impaired myelination of axons.

We note that there are some striking similarities between this body of work and recent work from the autism field. Autistic human listeners, as well as animal models of autism (the Fragile X mouse model, representing the most common monogenetic cause for autism), also have reduced ABR wave III[58,59]. Moreover, MNTB afferent axons from Fragile X mice show a similar reduction of myelination as we show here for aging[39]. Additionally, the same Fragile X mice also have an increased population of immature oligodendrocytes[39]. While synaptophathy and hidden hearing loss may play a role in the aging population, it is less likely this mechanism would also be active in the Fragile X mice, which are all young adults. In Fragile X, the underlying mechanism would more likely be impaired development, leading to diminished oligodendrocyte maturation, resulting in incorrect myelination of the axon bundle. The overall outcome is similar, since both autistic and aging listeners experience similar sound localization deficits and cocktail party performance deficits, while also having the same compromised temporal fidelity in MNTB afferent pathways.

MATERIALS AND METHODS

All animal procedures conducted in this study were reviewed and approved by the Institutional Animal Care and Use Committee (IACUC) of the University of Colorado Anschutz Medical Campus, under permit number 00617, and followed all OLAW and National Institutes of Health (NIH) standards for the humane treatment of laboratory animals.

Animals

A total of 17 gerbils, which were raised in-house at the CU Anschutz colony were utilized for these experiments. Animals from both sexes were used in the experiments for young (68 ± 3 days) and old (2 years 8 month, 1034d ±1 month). The exact number of animals used is listed in the figure legends for each experiment but ranged from 2-10 for each group and were between P65-P1100 (postnatal day).

Auditory brainstem response (ABR) acquisition

ABR recordings were carried out following procedures similar to those detailed in previous studies[60,61]. Briefly, gerbils were anesthetized using a combination of 100 mg/kg ketamine and 10 mg/kg xylazine, then placed on a heating pad inside a small soundproof chamber. The stimuli presentation, generation, and recording of evoked potentials were managed through custom Python software interfacing with an RME Fireface UCX Sound Card (REM audio, Haimhausen, Germany) operating at a sampling rate of 44.1 kHz. Stimuli were delivered via calibrated Etymotic ER10B ear coupling tubes and ER2 earphones (Etymotic, Elk Grove Village, IL, USA) using standard sound delivery tubes. Evoked potentials were recorded using platinum subdermal needle electrodes simultaneously placed at the apex and behind each pinna (active), referenced to the nape of the neck, grounded with a hind leg ground channel. The signals were then amplified, digitized, and processed for output using a range of specialized equipment including a Tucker Davis Technologies (TDT) low-impedance head stage (RA4LI), preamplifier (RA4PA), and digital amplifier (x10,000), along with a multi-input/output processor (RZ5) (Tucker-Davis Technologies, Alachua, FL, USA).

ABRs were elicited in response to 500 repetitions of sound stimuli consisting of 0.2 ms monaural (left and right) and binaural complex clicks with interstimulus intervals of 35 ± 5ms (mean ± SD). The responses were initially recorded for 90 dB SPL stimulus presentations and then gradually decreased in 10 dB SPL steps until the threshold level was reached. The threshold was defined as the average of the minimally detectable waveform and the next dB SPL step where a discernible ABR signal emerged in any of the three recorded channels.

ABR analysis

The recorded raw ABR traces were first band-pass filtered with a 100-3000 Hz 2nd order Butterworth filter, and then smoothed and detrended using a Savitzky-Golay filter. Wave peaks were automatically detected and labeled by finding the local maxima on the processed ABR traces,

and the wave labels were then inspected and adjusted if misclassified. All labeled peaks were quantified by the peak height, the peak half-width, and the peak latency.

Click ABR thresholds were estimated using two different approaches. For the objective estimation method, the cross-correlation (xCorr) of ABR traces between adjacent sound levels was calculated. The xCorr thresholds were computed by fitting the correlation-coefficient vs. sound level data to the sigmoid function[62]. For the conventional estimation method, the peak thresholds were determined by the sound level at 10 dB SPL below the minimum sound level that elicited visually detectable wave peaks. Researchers analyzing the ABR data were blinded to the animal and group information.

Tissue Preparation

Gerbils were euthanized via an overdose of pentobarbital (120 mg/kg body weight Fatal+, Vortech Pharmeceuticals, Dearborn, MI, USA and subsequently transcardially perfused with phosphate-buffered saline (PBS; containing 137 mM NaCl, 2.7 mM KCl, 1.76 mM KH2PO4, 10 mM Na2HPO4, Sigma-Aldrich) followed by 4% paraformaldehyde (PFA). Following perfusion, the animals were decapitated, and their brains were removed from the skull. The extracted brains were then post-fixed in 4% PFA overnight before being transferred to 30% sucrose for further processing. After the brains sank, they were washed three times in PBS to remove residual sucrose. Brains were then put in a mold in OCT compound (SAKURA 4583, Sakura Finetek, Torrance, CA, USA) and left to freeze in a cryostat (Leica CM1950, Leica Biosystems, Nussloch, Germany) for 20 minutes. The brainstem was sliced to 50 microns for CARS imaging and IHC (Immunohistochemistry). Slices were collected starting before the 7th nerve.

For EM imaging, brainstems from six animals were embedded in 4% agarose (in PBS) immediately following perfusion. Brains were coronally sliced at 800 µm using a Vibratome (Leica VT1000s), with subsequent division through the midline. One half of the brainstem was processed for CARS and IHC; the other half was fixed in 2.5% glutaraldehyde, 2% PFA, and 0.1 M cacodylate buffer (pH 7.4) for 24 hours. The tissue was rinsed in cacodylate buffer (recipe) and immersed two times in a mixture of 1% osmium and 0.8% potassium ferrocyanide (Sigma Chemical), each for 1.5 hours. Following rinses in water, the tissue was stained with 4% uranyl acetate in 50% ethanol for 2 hours. The tissue was then dehydrated through a graded series of ethanol, embedded in Embed812 resin (Electron Microscopy Sciences, Hatfield, PA, USA), and cured for 24 hours at 60°C. Ultra-thin sections (65 nm) were cut with a diamond knife (Diatome, Quakertown, PA, USAon a UC7 ultramicrotome (Leica Microsystems, Wetzlar, Germany) and collected on 200 mesh copper grids for analysis. Images were acquired on a Tecnai T12 transmission electron microscope (ThermoFisher Scientific, Waltham, MA, USA) equipped with a LaB6 source at 120kV, using an NS15 (15 Mpix) camera (AMT Imaging, Woburn, MA, USA).

For myelination analysis with CARS (Coherent Anti-stokes Raman Spectroscopy) microscopy, two to five slices per brain were stained with Nissl (Neurotrace 425/435 Blue-Fluorescent Nissl Stain, Invitrogen, 1:200), in antibody media (AB media: 0.1 M phosphate buffer

(PB: 50 mM KH2PO4, 150 mM Na2HPO4), 150 mM NaCl, 3 mM Triton-X, 1% bovine serum albumin (BSA)) for 30 minutes at room temperature on a standard laboratory shaker, then stored free-floating at 4°C until imaged.

Immunohistochemistry

For staining oligodendrocytes, six to eight free-floating sections from each brain were submerged in L.A.B. solution (Polysciences, Warrington, PA, USA) for 10 minutes to expose epitopes. Sections were then washed twice in PBS and blocked in a solution containing 0.3% Triton-X, 5% normal goat serum (NGS), and PBS for 1 hour on a laboratory shaker. After blocking, sections were stained overnight with primary antibodies (table 1): rabbit anti-Aspartoacylase (GeneTex, Irvine, CA, USA 1:1,000) and mouse Sox-10 (Santa Cruz Biotechnology, Santa Cruz, CA, USA, sc-365692, 1:500) in blocking solution with 1% NGS. The sections were then washed three times in PBS (10 minutes each wash) and incubated for 2 hours in secondary antibodies (table 2) (diluted in blocking solution with 1% NGS). After three additional PBS washes (5 minutes each), sections were stained with Neurotrace 425/435 Blue-Fluorescent Nissl Stain (ThermoFisher Scientific, Waltham MA, USA, 1:200) in antibody media (0.1 M phosphate buffer, 150 mM NaCl, 3 mM Triton-X, 1% BSA) for 30 minutes. Finally, the stained sections were washed briefly in PBS, slide-mounted with Fluoromount-G (Southern Biotech, Birmingham, AL, USA), and stored at 4°C. All antibody labeling was performed at room temperature.

Antibody	Immunogen	Manufacturer, species, mono or polyclonal, cat. or lot no., RRID	Concentration
Aspartoacylase (ASPA)	Recombinant protein encompassing a sequence within the center region of human Aspartoacylase	GeneTex (Irvine, CA, United States), rabbit polyclonal, GTX113389, RRID:AB_10727411	1:1,000
Sox-10 (A-2)	An epitope between amino acids 2-29 at the N-terminus of Sox-10 protein.	Santa Cruz Biotechnology, (Dallas, TX, United States), mouse monoclonal, sc-365692; RRID:AB_10844002	1:500

Table 1. *Primary antibodies used in immunofluorescence.*

Catalog No., RRID	Manufacturer	Reactivity	Conjugate	Concentration
A-21428, AB_2535849	Invitrogen	Goat anti-Rabbit IgG (H + L)	Alexa Fluor 555	1:500
A-21235, AB_2535804	Invitrogen	Goat anti-Mouse IgG (H + L)	Alexa Fluor 647	1:500

Table 2. *Secondary antibodies used in immunofluorescence.*

Antibody Characterization

The primary antibody for mature oligodendrocytes, Aspartoacylase (ASPA, 1:1,000, GeneTex, Irvine, CA, USA; GTX113389), is a rabbit polyclonal antibody specific to mature oligodendrocytes (OLs). This antibody targets a recombinant protein sequence within the center region of human aspartoacylase, which converts N-acetyl-L-aspartic acid (NAA) to aspartate and acetate, aiding in white matter maintenance[63]. It has been validated for labeling mature OLs in mouse cerebral cortex through protein overexpression and western blot analysis[64,65] as well as in

our previous study of the auditory brainstem[39] The Sox-10 antibody [Sox-10 (A-2), 1:500, Santa Cruz Biotechnology Santa Cruz, CA, USA, sc-365692] is a mouse monoclonal antibody specific to an epitope between amino acids 2–29 at the N-terminus of the human Sox-10 gene. This antibody labels the entire oligodendrocyte lineage (OPCs and OLs) and has been shown to specifically mark these cells in the CNS and mouse brains[66–68]. Both primary antibodies were visualized using fluorescent-conjugated secondary antibodies (listed in Table 2).

Imaging

Brainstem slides for immunofluorescence were imaged using an Olympus FV1000 confocal microscope (Olympus) with 488, 543, and 635 nm lasers. The MNTB was identified by its trapezoidal morphology and cell size, and z-stacks were taken with a 20x objective (UPLSAPO20X, Olympus Life Science, Waltham, MA, USA NA 0.75) to visualize the entire nucleus. The nucleus was divided into medial, central, and lateral regions, following[43]. Briefly, the MNTB was digitally extracted using FIJI software, and the tonotopic axis was estimated by drawing a dorsomedial-to-ventrolateral line through the nucleus. This line was measured and divided into thirds with perpendicular lines to delineate the regions.

For CARS microscopy, brainstem sections were imaged using an Olympus FV-1000 with non-descanned detectors in both forward and epi CARS directions. Sections were placed in a culture dish with a coverslip bottom and held down by a custom glass weight. Z-stacks were taken with an Olympus 30x, 1.05 NA silicone oil objective (Olympus Life Science, Waltham, MA, USA) to collect the CARS signal in the epi direction. Signal in the forward direction was collected through an Olympus 0.55 NA condenser. An APE picoEmerald OPO laser system (APE, Berlin, Germany) was used to generate the pump/probe beam which is tunable from 770nm to 990nm, and the fixed wavelength Stokes beam at 1031 nm. Myelin was visualized by imaging the CH2 stretch-mode at 2,845 $cm^{-1;}$ the pump/probe beam was set to 797.2 nm, resulting in a CARS signal at 649.8 nm. The tunable pump/probe beam also generates two-photon excitation fluorescence which was separated from the CARS signal by a dichroic mirror and detected in a separate channel by the non-descanned detector (NDD) unit in epi-direction.

Four brains from young and two from old gerbils were processed and imaged with electron microscopy. Sections for EM were first imaged on a compound microscope to identify the MNTB by cell size, shape, and location in parasagittal slices. Once located, slices were imaged on a FEI Tecnai G2 transmission electron microscope (ThermoFisher Scientific, Waltham, MA, USA) with an AMT digital camera (AMT Imaging, Woburn, MA, USA).

Cell Counting

Quantification of OL's and entire OL lineage (OPCs and OLs) was performed as follows. In FIJI, each stack was brightened, the background subtracted, the image scaled and the MNTB

digitally extracted. Each slice of the SOX10 channel was thresholded and the morphology of the (OL + OPC) cells within the MNTB was identified with FIJI particle analysis. Some cells were visible on neighboring slices. To prevent overcounting, we identified and combined close (less than 4 micron apart) particles into single cells with a custom-made script (Igor Pro). Masks were calculated for each cell, and the mean signal on the ASPA channel within the mask was recorded.

Myelination Analysis

Myelin diameter was measured from CARS images using FIJI software. The line tool was used to measure the fiber diameter for 30 axons per image (Figure 5A). Due to resolution limitations, CARS images could not be used to quantify myelin thickness or g-ratios.

For EM images, cross-sections of myelinated fibers were blindly sampled through visual inspection. The myelin layers were semi-automatically segmented by active contours. Dead axons with incomplete and loose lamellae as well as small fibers with diameter less than 1 micrometer were eliminated for the following analysis. The morphological metrics, including fiber diameter, myelin thickness, axon diameter, and g-ratio (ratio between axon diameter and fiber diameter) of sampled myelinated fibers were extracted by using AxonDeepSeg software (Figure 5B)[69]. The conduction velocity of quantified fibers was estimated by simulating the multi-compartment axon model of Halter and Clark[70] implemented in the myelinated axon model[18,42].

Statistical Analysis

For CARS and confocal images, we employed ANOVA followed by the Tukey test to measure statistical differences between MNTB regions in young and aging groups. Student's t-test was used to measure statistical differences in each MNTB subregion between the two age groups. Reported p values were corrected for multiple comparisons using the Bonferroni correction. For metrics quantified from ABRs and EM images, the two-sided Mann-Whiteny U test was utilized due to its robustness in handling uneven sample sizes and skewed distributions.

REFERENCES

1. Arvin, B., Prepageran, N. & Raman, R. "High Frequency Presbycusis"–Is There an Earlier Onset? *Indian J Otolaryngol Head Neck Surg* **65**, 480–484 (2013).
2. Huang, Q. & Tang, J. Age-related hearing loss or presbycusis. *Eur Arch Otorhinolaryngol* **267**, 1179–1191 (2010).
3. López-Torres Hidalgo, J. *et al.* Functional status of elderly people with hearing loss. *Archives of Gerontology and Geriatrics* **49**, 88–92 (2009).
4. Veras, R. P. & Mattos, L. C. Audiologia do envelhecimento: revisão da literatura e perspectivas atuais. *Rev. Bras. Otorrinolaringol.* **73**, 128–134 (2007).
5. Ciorba, A., Bianchini, C., Pelucchi, S. & Pastore, A. The impact of hearing loss on the quality of life of elderly adults. *CIA* 159 (2012) doi:10.2147/CIA.S26059.
6. Ying, G., Zhao, G., Xu, X., Su, S. & Xie, X. Association of age-related hearing loss with cognitive impairment and dementia: an umbrella review. *Front. Aging Neurosci.* **15**, 1241224 (2023).
7. Carrijo, M. F. *et al.* Relationship between depressive symptoms, social isolation, visual complaints and hearing loss in middle-aged and older adults. *Psychiatriki* **34**, 29--35 (2023).
8. Brotto, D. *et al.* Age-related changes in auditory perception. Hearing loss in the elderly: aging ear or aging brain? *Aging Clin Exp Res* **35**, 2349–2354 (2023).
9. Johnson, J. C. S. *et al.* Hearing and dementia: from ears to brain. *Brain* **144**, 391–401 (2021).
10. Wang, J. & Puel, J.-L. Presbycusis: An Update on Cochlear Mechanisms and Therapies. *JCM* **9**, 218 (2020).
11. Briley, P. M. & Summerfield, A. Q. Age-related deterioration of the representation of space in human auditory cortex. *Neurobiology of Aging* **35**, 633–644 (2014).
12. Ruggles, D., Bharadwaj, H. & Shinn-Cunningham, B. G. Normal hearing is not enough to guarantee robust encoding of suprathreshold features important in everyday communication. *Proc. Natl. Acad. Sci. U.S.A.* **108**, 15516–15521 (2011).
13. Shamma, S. On the Emergence and Awareness of Auditory Objects. *PLoS Biol* **6**, e155 (2008).
14. Dubno, J. R., Ahlstrom, J. B. & Horwitz, A. R. Binaural Advantage for Younger and Older Adults With Normal Hearing. *J Speech Lang Hear Res* **51**, 539–556 (2008).
15. Rayleigh, Lord. XII. *On our perception of sound direction. The London, Edinburgh, and Dublin Philosophical Magazine and Journal of Science* **13**, 214–232 (1907).
16. Grothe, B., Pecka, M. & McAlpine, D. Mechanisms of Sound Localization in Mammals. *Physiological Reviews* **90**, 983–1012 (2010).
17. Trussell, L. O. Synaptic Mechanisms for Coding Timing in Auditory Neuron. *Annu. Rev. Physiol.* **61**, 477–496 (1999).
18. Ford, M. C. *et al.* Tuning of Ranvier node and internode properties in myelinated axons to adjust action potential timing. *Nat Commun* **6**, 8073 (2015).
19. Ford, M. C., Grothe, B. & Klug, A. Fenestration of the calyx of held occurs sequentially along the tonotopic axis, is influenced by afferent activity, and facilitates glutamate clearance. *J of Comparative Neurology* **514**, 92–106 (2009).
20. Stange-Marten, A. *et al.* Input timing for spatial processing is precisely tuned via constant synaptic delays and myelination patterns in the auditory brainstem. *Proc. Natl. Acad. Sci. U.S.A.* **114**, (2017).
21. Kim, T. S. & Chung, J. W. Evaluation of Age-Related Hearing Loss. *Korean J Audiol* **17**, 50 (2013).
22. Kim, J. H., Renden, R. & Von Gersdorff, H. Dysmyelination of Auditory Afferent Axons Increases the Jitter of Action Potential Timing during High-Frequency Firing. *J. Neurosci.* **33**, 9402–9407 (2013).
23. Kim, K. *et al.* Artifact-free and high-temporal-resolution in vivo opto-electrophysiology with microLED optoelectrodes. *Nature Communications* **11**, 2063 (2020).
24. Nabel, A. L. *et al.* Development of myelination and axon diameter for fast and precise action potential conductance. *Glia* **72**, 794–808 (2024).

25. Sinclair, J. L. *et al.* Sound-Evoked Activity Influences Myelination of Brainstem Axons in the Trapezoid Body. *J. Neurosci.* **37**, 8239–8255 (2017).
26. Peters, A. & Sethares, C. Aging and the myelinated fibers in prefrontal cortex and corpus callosum of the monkey. *J of Comparative Neurology* **442**, 277–291 (2002).
27. Ibañez, S., Sengupta, N., Luebke, J. I., Wimmer, K. & Weaver, C. M. Myelin dystrophy in the aging prefrontal cortex leads to impaired signal transmission and working memory decline: a multiscale computational study. Preprint at https://doi.org/10.1101/2023.08.30.555476 (2023).
28. Haykin, S. & Chen, Z. The Cocktail Party Problem. *Neural Computation* **17**, 1875–1902 (2005).
29. Cherry, E. C. Some experiments on the recognition of speech, with one and with two ears. *The Journal of the Acoustical Society of America* **25**, 975--979 (1953).
30. Blauert, J. Spatial hearing: the psychophysics of human sound localization. in (MIT press, 1997).
31. Xie, R. Transmission of auditory sensory information decreases in rate and temporal precision at the endbulb of Held synapse during age-related hearing loss. *Journal of Neurophysiology* **116**, 2695–2705 (2016).
32. Šuta, D., Rybalko, N., Pelánová, J., Popelář, J. & Syka, J. Age-related changes in auditory temporal processing in the rat. *Experimental Gerontology* **46**, 739–746 (2011).
33. Ryan, A. Hearing sensitivity of the mongolian gerbil, Meriones unguiculatus. *The Journal of the Acoustical Society of America* **59**, 1222–1226 (1976).
34. Tarnowski, B. I., Schmiedt, R. A., Hellstrom, L. I., Lee, F. S. & Adams, J. C. Age-related changes in cochleas of mongolian gerbils. *Hearing Research* **54**, 123–134 (1991).
35. Keithley, E. M., Ryan, A. F. & Woolf, N. K. Spiral ganglion cell density in young and old gerbils. *Hearing Research* **38**, 125–133 (1989).
36. Curnow, E. & Wang, Y. New Animal Models for Understanding FMRP Functions and FXS Pathology. *Cells* **11**, 1628 (2022).
37. Wang, Z. *et al.* Functional Parameters of Prestin Are Not Correlated With the Best Hearing Frequency. *Front. Cell Dev. Biol.* **9**, 638530 (2021).
38. McCullagh, E. A., Poleg, S., Stich, D., Moldovan, R. & Klug, A. Coherent Anti-Stokes Raman Spectroscopy (CARS) Application for Imaging Myelination in Brain Slices. *JoVE* 64013 (2022) doi:10.3791/64013.
39. Lucas, A., Poleg, S., Klug, A. & McCullagh, E. A. Myelination Deficits in the Auditory Brainstem of a Mouse Model of Fragile X Syndrome. *Front. Neurosci.* **15**, 772943 (2021).
40. Stancu, M. *et al.* Ambient sound stimulation tunes axonal conduction velocity by regulating radial growth of myelin on an individual, axon-by-axon basis. *Proc. Natl. Acad. Sci. U.S.A.* **121**, e2316439121 (2024).
41. Hill, R. A., Li, A. M. & Grutzendler, J. Lifelong cortical myelin plasticity and age-related degeneration in the live mammalian brain. *Nat Neurosci* **21**, 683–695 (2018).
42. Arancibia-Cárcamo, I. L. *et al.* Node of Ranvier length as a potential regulator of myelinated axon conduction speed. *eLife* **6**, e23329 (2017).
43. Weatherstone, J. H. *et al.* Maintenance of neuronal size gradient in MNTB requires sound-evoked activity. *Journal of Neurophysiology* **117**, 756–766 (2017).
44. Diao, T., Ma, X., Fang, X., Duan, M. & Yu, L. Compensation in neuro-system related to age-related hearing loss. *Acta Oto-Laryngologica* **144**, 30–34 (2024).
45. Grothe, B. New roles for synaptic inhibition in sound localization. *Nat Rev Neurosci* **4**, 540–550 (2003).
46. Von Gersdorff, H. & Borst, J. G. G. Short-term plasticity at the calyx of held. *Nat Rev Neurosci* **3**, 53–64 (2002).
47. Held, H. Die centrale gehörleitung. *Arch Anat Physiol Anat Abt* **17**, (1893).
48. Smith, P. H., Joris, P. X. & Yin, T. C. T. Anatomy and Physiology of Principal Cells of the Medial Nucleus of the Trapezoid Body (MNTB) of the Cat. *Journal of Neurophysiology* **79**, 3127–3142 (1998).

49. Leão, R. N., Leão, R. M., Da Costa, L. F., Rock Levinson, S. & Walmsley, B. A novel role for MNTB neuron dendrites in regulating action potential amplitude and cell excitability during repetitive firing. *Eur J of Neuroscience* **27**, 3095–3108 (2008).
50. Kuwabara, N. & Zook, J. M. Classification of the principal cells of the medial nucleus of the trapezoid body. *J of Comparative Neurology* **314**, 707–720 (1991).
51. Spangler, K. M., Warr, W. B. & Henkel, C. K. The projections of principal cells of the medial nucleus of the trapezoid body in the cat. *J of Comparative Neurology* **238**, 249–262 (1985).
52. Moore, M. & Caspary, D. Strychnine blocks binaural inhibition in lateral superior olivary neurons. *J. Neurosci.* **3**, 237–242 (1983).
53. Peters, A. The effects of normal aging on myelinated nerve fibers in monkey central nervous system. *Front. Neuroanat.* **3**, (2009).
54. Spitzer, S. O. *et al.* Oligodendrocyte Progenitor Cells Become Regionally Diverse and Heterogeneous with Age. *Neuron* **101**, 459-471.e5 (2019).
55. Furman, A. C., Kujawa, S. G. & Liberman, M. C. Noise-induced cochlear neuropathy is selective for fibers with low spontaneous rates. *Journal of Neurophysiology* **110**, 577–586 (2013).
56. Viana, L. M. *et al.* Cochlear neuropathy in human presbycusis: Confocal analysis of hidden hearing loss in post-mortem tissue. *Hearing Research* **327**, 78–88 (2015).
57. Gould, E. & Kim, J. H. SCN2A contributes to oligodendroglia excitability and development in the mammalian brain. *Cell Reports* **36**, 109653 (2021).
58. ElMoazen, D., Sobhy, O., Abdou, R. & AbdelMotaleb, H. Binaural interaction component of the auditory brainstem response in children with autism spectrum disorder. *International Journal of Pediatric Otorhinolaryngology* **131**, 109850 (2020).
59. McCullagh, E. A., Salcedo, E., Huntsman, M. M. & Klug, A. Tonotopic alterations in inhibitory input to the medial nucleus of the trapezoid body in a mouse model of Fragile X syndrome. *J of Comparative Neurology* **525**, 3543–3562 (2017).
60. McCullagh, E. A. *et al.* Characterization of Auditory and Binaural Spatial Hearing in a Fragile X Syndrome Mouse Model. *eNeuro* **7**, ENEURO.0300-19.2019 (2020).
61. Benichoux, V., Ferber, A., Hunt, S., Hughes, E. & Tollin, D. Across Species "Natural Ablation" Reveals the Brainstem Source of a Noninvasive Biomarker of Binaural Hearing. *J. Neurosci.* **38**, 8563–8573 (2018).
62. Suthakar, K. & Liberman, M. C. A simple algorithm for objective threshold determination of auditory brainstem responses. *Hearing Research* **381**, 107782 (2019).
63. Bitto, E., Bingman, C. A., Wesenberg, G. E., McCoy, J. G. & Phillips, G. N. Structure of aspartoacylase, the brain enzyme impaired in Canavan disease. *Proc. Natl. Acad. Sci. U.S.A.* **104**, 456–461 (2007).
64. Larson, V. A. *et al.* Oligodendrocytes control potassium accumulation in white matter and seizure susceptibility. *eLife* **7**, e34829 (2018).
65. Orthmann-Murphy, J. *et al.* Remyelination alters the pattern of myelin in the cerebral cortex. *eLife* **9**, e56621 (2020).
66. Zuo, H. *et al.* Age-Dependent Decline in Fate Switch from NG2 Cells to Astrocytes After Olig2 Deletion. *J. Neurosci.* **38**, 2359–2371 (2018).
67. Barak, B. *et al.* Neuronal deletion of Gtf2i, associated with Williams syndrome, causes behavioral and myelin alterations rescuable by a remyelinating drug. *Nat Neurosci* **22**, 700–708 (2019).
68. Imamura, O., Arai, M., Dateki, M., Oishi, K. & Takishima, K. Donepezil-induced oligodendrocyte differentiation is mediated through estrogen receptors. *Journal of Neurochemistry* **155**, 494–507 (2020).
69. Zaimi, A. *et al.* AxonDeepSeg: automatic axon and myelin segmentation from microscopy data using convolutional neural networks. *Sci Rep* **8**, 3816 (2018).
70. Halter, J. A. & Clark, J. W. A distributed-parameter model of the myelinated nerve fiber. *Journal of Theoretical Biology* **148**, 345–382 (1991).

71. Joris, P *et al*. Enhancement of neural synchronization in the anteroventral cochlear nucleus I. Responses to tones at the characteristic frequency. *J. Neurophysiol* **71**, 1022-1036 (1994).
72. Budak, M *et al*. Binaural Processing Deficits Due to Synaptopathy and Myelin Deficits. *Front. Neural Circuits* **16**, 856926 (2022).
73. Kang, SH e*t al.* Degeneration and impaired regeneration of gray matter oligodendrocytes in amyotrophic lateral sclerosis. *Nature Neuroscience* **16**, 571-579 (2013).